



*Institute of Paper Science and Technology
Atlanta, Georgia*

IPST Technical Paper Series Number 655

Observations of the Bubble Dynamics in a Pulp Suspension Using Flash X-Ray Radiography

T.J. Heindel and J.L. Monefeldt

June 1997

Submitted to
1997 TAPPI Engineering & Papermakers Conference
Nashville, Tennessee
October 6–9, 1997

Copyright© 1997 by the Institute of Paper Science and Technology

For Members Only

INSTITUTE OF PAPER SCIENCE AND TECHNOLOGY PURPOSE AND MISSIONS

The Institute of Paper Science and Technology is a unique organization whose charitable, educational, and scientific purpose evolves from the singular relationship between the Institute and the pulp and paper industry which has existed since 1929. The purpose of the Institute is fulfilled through three missions, which are:

- to provide high quality students with a multidisciplinary graduate educational experience which is of the highest standard of excellence recognized by the national academic community and which enables them to perform to their maximum potential in a society with a technological base; and
- to sustain an international position of leadership in dynamic scientific research which is participated in by both students and faculty and which is focused on areas of significance to the pulp and paper industry; and
- to contribute to the economic and technical well-being of the nation through innovative educational, informational, and technical services.

ACCREDITATION

The Institute of Paper Science and Technology is accredited by the Commission on Colleges of the Southern Association of Colleges and Schools to award the Master of Science and Doctor of Philosophy degrees.

NOTICE AND DISCLAIMER

The Institute of Paper Science and Technology (IPST) has provided a high standard of professional service and has put forth its best efforts within the time and funds available for this project. The information and conclusions are advisory and are intended only for internal use by any company who may receive this report. Each company must decide for itself the best approach to solving any problems it may have and how, or whether, this reported information should be considered in its approach.

IPST does not recommend particular products, procedures, materials, or service. These are included only in the interest of completeness within a laboratory context and budgetary constraint. Actual products, procedures, materials, and services used may differ and are peculiar to the operations of each company.

In no event shall IPST or its employees and agents have any obligation or liability for damages including, but not limited to, consequential damages arising out of or in connection with any company's use of or inability to use the reported information. IPST provides no warranty or guaranty of results.

The Institute of Paper Science and Technology assures equal opportunity to all qualified persons without regard to race, color, religion, sex, national origin, age, disability, marital status, or Vietnam era veterans status in the admission to, participation in, treatment of, or employment in the programs and activities which the Institute operates.

OBSERVATIONS OF THE BUBBLE DYNAMICS IN A PULP SUSPENSION USING FLASH X-RAY RADIOGRAPHY

Theodore J. Heindel and James L. Monefeldt[†]
 Engineering Division
 Institute of Paper Science and Technology
 Atlanta, GA 30318

ABSTRACT

A greater understanding of the bubble dynamics in an air/water/fiber suspension is important to many paper processing areas such as flotation deinking and gaseous bleaching. However, using conventional visualization techniques to view gas bubbles in wood suspensions at consistencies relevant to the paper industry is nearly impossible because these systems are opaque. Therefore, alternative tools and techniques must be developed to characterize the bubble behavior in these complex systems.

In this study, flash x-ray radiography (FXR) is used to visualize air flows in a suspension of unprinted newsprint (ONP) at various consistencies and air injection rates. FXR provides stop-motion images of air bubbles rising through the opaque ONP suspension because air has a significantly different x-ray attenuation coefficient compared to water, while wood pulp and water have similar attenuation coefficients. Qualitative observations of these air/water/fiber flow conditions are reported and compared to those obtained in a simple air/water system. The radiographic images reveal that gas flow characteristics are substantially altered in the presence of fibers, implying that conclusions drawn in an air/water system may be drastically different from those actually obtained in an air/water/fiber system.

KEY WORDS:

flash x-ray radiography, bubble dynamics, flotation deinking, fluid mechanics, flow visualization

INTRODUCTION

Improved understanding of bubble rise and coalescence characteristics is important to many areas in the pulp and paper industry. One such area relevant to wastepaper processing, called flotation deinking, utilizes air bubbles to remove hydrophobic particles between approximately 20 to 300 μm in diameter from wastepaper slurries composed of

water, fiber, and other contaminant particles [1, 2]. Air bubbles are introduced into the system where the hydrophobic particles attach to the hydrophobic bubble surface. As the bubbles rise, they carry the contaminants to the surface where they are skimmed, leaving clean fiber behind to be used as recycled material. Bubble behavior in this system is very important because it has a direct effect on the contaminant removal efficiency. For example, a bubble must be large enough to produce a sufficient buoyant force to rise through the fiber network. However, if the bubble is too large, overall bubble surface area will be significantly reduced for a given total air volume, which reduces the area to which contaminant particles can attach. Additionally, large bubbles may reduce flotation efficiency by promoting the formation of discrete regions in the suspension where the majority of the air rises (defined as channeling), leaving some regions deficient of air bubbles. A second process common in paper processing comprising gas, water, and fiber involves gaseous fiber bleaching where, for example, ozone is introduced into a 1-3% consistency wood pulp suspension [3]. The ozone carrier gas must be well mixed with the wood fibers to ensure uniform bleaching reactions. Ideally, a homogeneous system would provide more efficient flotation and bleaching than a heterogeneous system. However, a systematic flow regime study has yet to be performed due to the complexities of this system. Furthermore, other parameters important for optimizing these processes, such as bubble size and bubble rise velocity, are not known for actual operating consistencies typically employed in flotation deinking or bleaching.

Methods to record bubble size, bubble rise velocity, and other multiphase flow parameters have been described in the literature [4-8]. These methods typically involve optical visualization and/or laser doppler techniques. When the system is translucent or opaque, common in many gas/liquid systems, optical and laser techniques can only be utilized near the system boundaries (i.e., walls), if at all. However, the information gathered near the system boundaries can be influenced by the confining wall and may not be representative of the true conditions within the bulk flow. For these systems, information concerning the bulk flow may be obtained by inserting selected probes into the system to measure parameters of interest. Difficulties may arise with traditional experimental tools, like high-speed video, laser doppler velocimetry, electrical resistivity probes, or optical probes, when the multiphase system is translucent or opaque and has one phase that may interact with, or impede the performance of, intrusive probes, such as gas/liquid/fiber systems involved in flotation deinking and gaseous bleaching.

[†] Current Address: Champion International Corporation
 Courtland, Alabama

Attempts to visualize these complex fiber suspensions have been conducted by Walmsley [9] where water was replaced by clove oil to produce a system that had the same refractive index as wood fiber. However, the applicability of these results to air/water/fiber systems is unknown. Additional experiments have been performed to measure bubble size in dilute fiber systems less than 0.5% consistency by weight [10], but extension to higher consistency systems has yet to be published.

Radiation techniques offer the ability to penetrate opaque flows without inserting flow-altering probes into the system. Lindsay et al. [11] utilized γ -ray densitometry to measure cord average void fractions (gas holdup) in two different test cells involving air, water, and ONP fiber. This technique involves recording, via a detector, the γ -rays emitted from a γ -source and transmitted through an object or region of interest over a period of time. However, local values were not recorded with the given setup and other parameters, such as bubble size, are difficult to obtain with this particular radiation technique. Therefore, additional tools and/or techniques must be developed. One such technique that can be used to visualize air bubble size and flow structures in an air/water/fiber system involves x-rays, called flash x-ray radiography.

FLASH X-RAY RADIOGRAPHY

Flash x-ray radiography (FXR) is an x-ray imaging process where an intense burst of radiation is produced for a fraction of a second to record dynamic events on film that may be obscured by dust, smoke, or light that would make conventional high-speed photography impossible. FXR also allows for images to be recorded of inclusions or voids inside opaque objects that are part of these dynamic events. Current areas where FXR is commonly utilized include high-velocity ballistics, explosives, weapons development, nondestructive testing, and medical and biological studies [12].

The fundamentals of FXR are similar to traditional x-ray radiography [12-14]. X-rays can range in energy from less than 0.1 keV to more than 100 MeV. High-energy x-rays are referred to as "hard" x-rays, and low-energy x-rays are described as "soft" x-rays. FXR typically consists of both hard and soft x-rays. Hard x-rays contain the short wavelength x-ray component and is required to penetrate thick objects or those with large object densities, whereas the soft x-ray component is comprised of longer wavelength x-rays and is necessary to enhance image contrast.

X-rays affect photographic emulsions in the same way visible light does. Therefore, a radiograph is a photographic record of an object produced on film exposed by the

penetration and scattering of x-rays through the object. Hence, a radiograph is a shadow picture of an object with lighter images associated with object areas of greatest density. The film is subsequently developed to view the image. The ratio of the dimensions of the object and image is the same as the ratio of the distances between the source and object and the source and film. Therefore, when the ratio of the distances between source and object and source and film is approximately 1, the x-ray image size is equivalent to the actual object size.

X-ray image quality is dependent on the contrast developed in the radiograph due to the x-ray attenuation characteristics of the materials in the system of interest. Contrast may be reduced by several independent mechanisms, some due to x-ray absorption, which is highly dependent on wavelength, others due to x-ray scattering. X-ray scatter (secondary x-rays) results in a general fogging of the film, which reduces the image sharpness, clarity, contrast, and resolution. Scattering may be reduced by passing the x-ray beam through a metal filter to reduce the amount of soft x-rays reaching the subject. The intensity of incident x-rays on the film can also be increased through the use of fluorescent intensifying screens, but the downside is they reduce the image sharpness. Photographic grain size also affects image quality. The fine-grain, high-contrast film requires longer x-ray exposure times than fine-grain, low-contrast film. Additionally, high-speed, high-contrast film has a larger grain size than low-speed, high-contrast film. Finally, a small x-ray source is essential to obtain good definition in a radiograph and reduce the penumbra effect [14]. In summary, optimal contrast is not easy to obtain, and each object/film/screen/filter combination must be analyzed by trial and error to determine conditions for the best sharpness, clarity, contrast, and resolution.

As described, FXR has the ability to penetrate fluids that are opaque and produce a permanent film record of high-speed events. In the area of multiphase fluid mechanics, FXR has been used to visualize vapor development from boiling in metal tubes under high pressures [15]. A specially designed thin-walled titanium test section was utilized, and FXR provided a visual record of the flow conditions within this opaque structure. This study was expanded to compare flash photography and FXR of air/water flows at high liquid flowrates taken at the same instant in time [16]. Good qualitative agreement was obtained between both image recording techniques. Additionally, at very high liquid flowrates, the images acquired by FXR were superior to those obtained by conventional flash photography because the x-rays "saw through" the complex light refraction and reflections caused by the flow. Rowe and Partridge [17] also used x-rays to visualize gas bubbles in a multiphase system. They investigated the effect of fluidized particle diameter on

air bubble velocity and size in fluidized beds composed of glass ballotini or natural silver sand.

The application of FXR to air/water/fiber flows is justified because water and wood fibers have similar densities, whereas the density of air is considerably different from water and wood fiber. Water also has a linear x-ray attenuation coefficient (a measure of x-ray absorption) three orders of magnitude larger than air, and a suspension of wood fiber and water should absorb x-rays in a similar manner, unless the water or fiber has been treated with special radioactive materials. Hence, water and wood fibers will absorb x-rays at a similar rate, but at a significantly different rate compared to air.

Imaging gas flows with FXR is compared to standard optical imaging in Fig. 1. In optical imaging (Fig. 1a), the continuous phase must be transparent for light rays to pass through it. A bubble surface will reflect the incident light rays. This reflection is viewed by the observer, camera, or video recorder and represents the actual bubble/fluid interface. When the continuous phase is translucent or opaque, optical observations become difficult, if not impossible. In contrast, x-rays are differentially absorbed by many materials. A given amount of x-rays, depending on the material, is also transmitted through the object and can be recorded on x-ray sensitive film located on the opposite side of the object from the incident x-rays. Therefore, if the continuous phase (i.e., a dilute water/fiber suspension) absorbs x-rays at one rate, but the discontinuous phase (i.e., air bubbles) absorbs x-rays at another, the difference can be recorded on film, and the resulting image represents the discontinuous phase. This is schematically shown in Fig. 1b where x-rays will pass through a given distance of air at a rate 1000 times more than through the same distance of water. Since an air bubble has a curved surface, the x-rays incident on the film will produce a gray-scale gradient from the bubble interior to the bubble edge. Hence, actual bubble sizes may be difficult to measure with FXR, but qualitative observations can easily be made.

Over the past 10 years, FXR has been used periodically to study areas relevant to the pulp and paper industry. Farrington used FXR to study high consistency forming [18], and demonstrated that FXR is a potentially powerful technique for the investigation of high-speed multiphase flows in general and concentrated fiber flows in particular. He extended this technique to investigate sheet formation and quality [19] and black liquor spray formation [20]. Triantafillopoulos and Farrington [21] further extended this technique to visualize flow phenomena in opaque coating applications. Finally, Zavaglia and Lindsay [22] applied FXR and an x-ray tracing fluid to visualize fluid motion during impulse drying. The commonality between these

processes is that the events of interest are typically high speed and the region of visual interest is obscured – ideal for application to FXR. In this study, FXR is used to visualize air flows in a suspension of unprinted newsprint (ONP) at various consistencies and flow rates. Qualitative observations of these air/water/fiber flow conditions are reported and compared to those obtained in a simple air/water system.

EXPERIMENTAL METHODS

The experimental setup used in this study is shown in Fig. 2. The x-ray unit was a 300 keV HP 43733A flash x-ray system (currently supported by Primex Physics International), which generates a 30 nanosecond x-ray pulse. The x-ray tube head was mounted in a locking vertical slide to allow x-ray exposures at various bubble column heights. A 3.25 mm aluminum filter was mounted directly in front of the x-ray source aperture to filter soft x-rays that promote scattering effects and result in fuzzy images [14]. The resulting hardened x-ray beam produced sharper images with less scattering. The entire system was housed in a 3.5 m × 4.5 m room lined with lead foil for safety considerations.

The planar bubble column, with interior dimensions 20 cm wide by 2 cm deep, was composed of face panes of 6.35 mm clear acrylic stock. The column was 1 m tall with lead numbers affixed to both sides to indicate the column height, which was recorded on film when x-rays were taken. Compressed air was injected into the base of the column through nine evenly spaced holes along the central axis of a 3.18 mm thick n-butyl rubber gasket. The holes were formed in the gasket with a 0.34 mm diameter drill bit and were self-sealing when the air pressure was removed. The rubber gasket also separated the bubble column from a conical air diffuser and allowed for the possibility of using different air injection patterns and/or hole sizes. Air flow was regulated with a Dixon air regulator and filter, and was measured with one of two Sierra Instruments mass flow meters, one covering air flow rates less than 1 slpm (standard liter per minute) and one covering air flow rates less than 40 slpm. The entire bubble column was mounted on a support stand with locking wheels to allow horizontal placement from the x-ray source.

A single 20 cm × 25.2 cm x-ray negative was exposed during the discharge of the x-ray unit. The x-ray film was either AGFA D8 or D6 Structurix film and was mounted in a film cassette between two Dupont Quanta Rapid Back PF intensifying screens. This was performed in a lightproof room where the x-ray negatives were also manually developed. X-ray film developing procedures are detailed in [23].

Each x-ray negative was exposed by attaching the film cassette to the back of the bubble column in the orientation and in one of three positions identified in Fig. 2, and then discharging the x-ray unit. A lead letter/number identification was taped to each cassette to permanently identify the image when exposed to radiation. The x-ray source was located in front of, and perpendicular to, the planar bubble column. All radiographs were taken at a source-to-film distance of 1.65 m and an object-to-film distance of 1.6 cm, ensuring negligible image magnification and distortion [13, 14]. The bubble column and x-ray tube were aligned using a laser pointer mounted on top of the x-ray tube such that the x-ray aperture was coincident with the center of the x-ray film.

The air/water system used in this study consisted of compressed and filtered building air and deionized water. Air/water/fiber systems were composed of deionized water and unprinted old newsprint (ONP). The old newsprint was reslushed following TAPPI method T 205 om-88 [24]; however, deionized water was used, and the disintegration was performed at 1.5% consistency. Three samples from this slurry were analyzed with a Kajaani FS-100 fiber length analyzer for fiber length characterization, yielding a weighted mean fiber length of 1.3 mm. Pulp slurries of 0.5% and 1.0% consistency were prepared by diluting samples of the 1.5% consistency stock with deionized water. Formaldehyde (37% solution) was added to the samples (2.0 cm³/l) to prevent biological degradation. It was assumed that this small amount of formaldehyde did not significantly affect the flow characteristics.

The bubble column was charged by filling it with the desired water/fiber slurry from the top until a slurry height of 80 cm was reached. This allowed for fluid expansion in the column once air was introduced into the system. The column was drained when not in use through a valved opening located on the column side near its base. After filling, the fiber suspension slowly separated over a period of hours if the system was not agitated. Therefore, a moderate air injection rate was maintained to keep the system well mixed. After an experiment was set up and the x-ray film was properly located, the air injection rate was adjusted to the desired level. A waiting period of 10-15 minutes allowed the flow to reach quasi-steady-state conditions (to be commented on in the next section), whereupon an x-ray was taken. A total of 176 x-rays were taken during this study.

Verification of the FXR technique to capture a true image of air bubbles rising through water was completed by Monefeldt [23] by comparing images acquired with high-speed video photography with those obtained at the same time (± 0.033 sec) using FXR. Very good qualitative

agreement was obtained and identical bubbles and bubble groups were identified on both the video and FXR images.

RESULTS

Flash x-rays of an air/water system and an air/water/fiber system at 0.5%, 1.0%, and 1.5% consistency were obtained at three locations in a planar bubble column over a range of volumetric air injection rates (∇) of $0.25 \text{ slpm} \leq \nabla \leq 30 \text{ slpm}$ (standard liters per minute). This corresponds to a superficial gas velocity of $0.10 \text{ cm/s} \leq u_g \leq 12.5 \text{ cm/s}$, where $u_g = \nabla/A_c$ with A_c representing the column cross-sectional area.

Air/Water Observations with FXR

Figure 3 displays composite radiographs obtained in an air/water system at three different air injection rates, where the arrows at the base of each column represent the relative locations of each air inlet hole. The x-rays of each column represent the composite of individual x-rays taken at one of three positions and at separate time intervals. Position 1 and Position 3 correspond to the bottom and top image, respectively. The gap between the channel bottom where the air is introduced and the beginning of the first image (Position 1) is due to the flange and bolts that are used to attach the column to the diffuser, preventing the film cassette from being placed any lower. The gaps between Positions 1 and 2 and Positions 2 and 3 are caused by the film cassette holder being fixed at specific column locations. The actual image that encompassed the column interior was $20 \text{ cm} \times 20 \text{ cm}$ with approximately 2.5 cm of film overhanging each side, which included the lead position indicators and radiograph identification label. The radiograph portions including the identification and location numbers have been removed from the images presented here to increase clarity. The radiographs, as shown in the format presented here, have some loss of detail as a result of electronic digitization and reduction, but the images are representative of the originals, which are available at the Institute of Paper Science and Technology. All observations are based on the original images.

Figure 3a corresponds to an air injection rate of $\nabla = 0.5$ slpm and shows discrete air bubbles rising through the water column in a well-dispersed fashion. This flow pattern is typically referred to as bubbly flow [25]. Upon close examination of each radiograph, the bubbles appear to be elliptical in shape with a major axis length between approximately 2 and 5 mm, indicating the bubbles are fairly uniform in size compared to other test conditions (i.e., Fig. 3c). The air/water patterns observed at $\nabla = 0.5$ slpm continue throughout the column height, with negligible evidence of bubble coalescence. These observations are also

confirmed by visual examination of the air/water flow characteristics before and after the radiographs were taken.

Increasing the air injection rate to $\nabla = 2.0$ slpm (Fig. 3b) results in the appearance of many more bubbles. Some of the bubbles appear to be clumped together in groups, and it is hypothesized that these bubble groups will coalesce to form a single larger bubble if the thin liquid film between the bubbles has sufficient time to thin and rupture before the bubbles break the surface. Additionally, some larger bubbles are also observed which are more than likely formed by the coalescence of these groups of smaller bubbles. Coalescence is further verified by the observations of more larger bubbles being recorded at Position 3 than at Position 1. Hence, they coalesce as they rise through the column. The flow regime associated with this air injection rate is still considered bubbly because the flow remains predominantly homogeneous.

At $\nabla = 15$ slpm (Fig. 3c), the flow is now considered to be churn-turbulent [25], characterized by a heterogeneous flow of rather large bubbles that form by the coalescence of smaller bubbles, with some smaller bubbles still present throughout the column. The large dark regions in these radiographs correspond to single large bubbles. Some are formed at the column base as the air is introduced into the column at these high air injection rates. Others form as the bubbles rise through the column and interact with each other in this highly turbulent flow. At these high air injection rates, backmixing is visually observed in the column, where large bubbles (that may span the 2 cm column depth) travel up the central region of the column in a serpentine pattern and smaller bubbles adjacent to the walls travel downward, trapped in the backmixed flow around the oscillating rising channels of air. The smaller bubbles are eventually caught in the rising bulk flow. Backmixing is not captured on the radiographs, nor is it recorded on photographs; however, it is possible to record this phenomenon by video analysis if the system is transparent.

Air/Water/0.5% ONP Observations with FXR

The bubble column flow characteristics begin to change when as little as 0.5% ONP fiber by weight is added to the air/water system. Figure 4a reveals the flow patterns for the air/water/0.5% ONP system with an air injection rate of $\nabla = 0.5$ slpm. The bubbles remain approximately the same size as those observed at 0% consistency (air/water flow only). The main difference between the 0% and 0.5% system at $\nabla = 0.5$ slpm is that at 0.5% ONP, the bubbles recorded on the radiographs are much more spherical than those observed at 0%. These differences are clearly evident in the original radiographs. The presence of fibers increases the effective viscosity of the suspension, reducing the bubble rise

velocity (i.e., the bubble Reynolds number), which produces bubbles that are more spherical [4].

When the air injection rate for this system is increased to $\nabla = 2$ slpm (Fig. 4b), more bubbles are present and the range of bubble sizes observed in the radiographs has increased considerably. Many small bubbles are still present, but more large bubbles are also observed and the flow could be considered to be beginning the transition from bubbly flow to churn-turbulent flow, termed transitional flow.

At $\nabla = 15$ slpm with 0.5% ONP (Fig. 4c), the flow is very turbulent and the bubble flow regime is churn-turbulent. There are many small bubbles present, but there are also a significant number of very large bubbles. The largest bubbles in Fig. 4c actually span the entire column width of 2 cm and rise in a central oscillating channel. The oscillations cause backmixing, which is not specifically captured on the radiographs, but is visually observed in the flow near the walls. Additionally, the many large bubbles that form at the base of the column due to the large influx of air coalesce with smaller bubbles and each other, forming even larger, but less numerous, bubbles towards the top of the column.

Air/Water/1.0% ONP Observations with FXR

Increasing the ONP consistency to 1% results in another significant change in the bubble characteristics. At an air injection rate of $\nabla = 0.5$ slpm (Fig. 5a), there are preferential regions at the base of the column (Position 1) where the air bubbles rise and other regions void of rising bubbles. This is a result of fiber network formation which restricts the rise of small bubbles. When a bubble is large enough to break through the fiber network, or a bubble finds a local region where no network exists, the bubbles rise. As they rise, they push the fiber aside creating local regions with a fiber consistency less than the average value of 1%, and other regions where the local consistency is greater than 1%. The locally low consistency regions have a low resistance to bubble rise, creating the preferential rise paths for the ascending bubbles. This phenomenon is typically termed channeling. Generally, the location of these preferential rise paths is not static due to the shifting of the fiber network caused by interaction with intermittent rising bubbles. For example, a small bubble may become trapped in a fiber network, but other rising bubbles may also get trapped and coalesce with the first bubble to form a resulting bubble large enough to break through the network. As it breaks through, the adjacent fibers are pushed aside, which may close a nearby preferential rise path and cause a new local fiber network to form. This new network will now trap bubbles in this region, and the process begins again.

Therefore, the overall flow conditions within the column are more likely to be quasi-steady-state in nature.

As the bubbles rise from Position 1 to Position 2 in Fig. 5a, they become more dispersed, but there are still regions in the column deficient of bubbles. Bubble dispersion continues toward the top of the column with Position 3 showing the most uniform bubbly flow of the three locations recorded at this air injection rate. Additionally, the bubbles at this consistency have a wider range of bubble sizes, with some of them being much larger than those observed at 0% and 0.5% consistency at the same air injection rate.

Figure 5b reveals the resulting flow patterns when the air injection rate is increased to $\nabla = 2.0$ slpm with an ONP consistency of 1%. Considerable coalescence takes place under these conditions and the resulting flow patterns are considered to be churn-turbulent. Therefore, increasing the fiber consistency results in an early transition to churn-turbulent flow.

When the air injection rate is further increased to $\nabla = 15$ slpm (Fig. 5c), a very chaotic flow pattern is recorded on the radiographs. Very large bubbles are observed due to the high coalescence rate. The resulting bubbles are also varied in shape due to the highly turbulent nature of the flow field. In addition to the very large bubbles, some very small bubbles are also recorded, but due to the small buoyant force associated with these bubbles, they are typically carried toward the column bottom due to backmixing. This is visually observed in the flow near the walls, but not specifically recorded in the radiographs.

Air/Water/1.5% ONP Observations with FXR

When the consistency is increased to 1.5% ONP, which is typically on the high side for flotation deinking, very unique flow patterns are observed. At $\nabla = 0.5$ slpm, discontinuous air channels are recorded at Position 1 (Fig. 6a). As they rise, they may form very large bubbles, as shown in Position 2, or they may break apart to form individual bubbles or bubble groupings. Large individual bubbles form when the air channel appears to be a single elongated air pocket. In contrast, the bubble groupings form, and may eventually disperse because of interaction with the fiber network, when the air channel is formed by a train of individual bubbles. In either case, the resulting flow pattern is heterogeneous and would not be considered to be bubbly flow.

At an air injection rate of $\nabla = 2.0$ slpm, Figure 6b displays that the majority of the recorded bubbles are rather large and very few small bubbles are observed in the radiographs.

Churn-turbulent flow conditions would prevail under these conditions.

When the air injection rate is increased to $\nabla = 15$ slpm with a consistency of 1.5% ONP, coalescence occurs very near the injection ports and very large bubbles are created near the column base (Fig. 6c). Small bubbles are still present in the radiographs, but they typically follow the fluid flow patterns due to the highly turbulent flow field. The turbulent flow field also results in uniquely-shaped large bubbles. Additionally, the large bubbles that form near the air injection ports coalesce to form even larger, less numerous bubbles at higher column locations.

Flow Pattern Influences

Bubbly flow is characterized by small, well-dispersed bubbles rising throughout the column width in a homogeneous pattern. In contrast, churn-turbulent flow is heterogeneous with large bubbles observed throughout the column width with the possibility of small bubbles interspersed with the large ones. The column flow conditions observed in this study changed from bubbly flow to churn-turbulent flow as the air injection rate and ONP consistency is increased. These changes are summarized in Fig. 7, where radiographs for Position 2 are presented for three different air injection rates and four different ONP consistencies. These radiographs clearly show the change from bubbly to churn-turbulent flow as the air injection rate is increased. The same effect occurs when the air injection rate is fixed (i.e., focus on 2 slpm) and the ONP consistency is increased.

Additionally, as the fiber consistency increases, the bubbles become larger and the air flow becomes more heterogeneous. Both of these effects are detrimental to efficient flotation deinking and gaseous bleaching. For example, increasing the bubble size reduces the overall surface area a contaminant can attach to during flotation deinking [26] and also decreases the mass transfer rate during gaseous bleaching [27].

Figure 7 also shows that the flow patterns and conditions observed in a simple air/water system are not those observed in an air/water/ONP fiber system when all other parameters are fixed. Therefore, general conclusions obtained in simplified multiphase flows should be applied with caution to fibrous multiphase flows.

CONCLUSIONS

In this study, flash x-ray radiography (FXR) is used to visualize air flows in a suspension of unprinted newsprint (ONP) at various consistencies and air injection rates.

Qualitative observations of these air/water/fiber flow conditions are reported and compared to those obtained in a simple air/water system. Increasing the air injection rate causes the flow conditions to change from bubbly to churn-turbulent. This trend is also observed by increasing ONP consistency while holding the air injection rate constant. Additionally, increasing the ONP consistency results in larger bubbles and promotes discrete regions in the column where the air bubbles rise (termed channeling). Finally, overall flow patterns are significantly influenced when ONP fibers are added to an air/water system. Therefore, expected bubble characteristics and flow conditions in flotation deinking and gaseous bleaching systems will not be the same as those observed in simplified air/water systems.

REFERENCES

- [1] McCool, M.A., "Flotation Deinking," *Secondary Fiber Recycling*. R.J. Spangenberg, Ed., Atlanta, TAPPI PRESS, 141-162 (1993).
- [2] Ferguson, L.D., "Flotation Deinking Technology," *1995 Deinking Short Course*, Vancouver, WA, TAPPI PRESS, Chapter 10 (June 4-7, 1995).
- [3] Lindholm, C.-A., "Effect of Heterogeneity in Pulp Bleaching with Ozone," *Paperi ja Puu*, **68**(4): 283-290 (1986).
- [4] Clift, R., Grace, J.R., and Weber, M.E., *Bubble, Drops, and Particles*, Academic Press, New York, 1978.
- [5] Hetsroni, G., Ed., *Handbook of Multiphase Systems*, Hemisphere Publishing Corp., New York, 1982.
- [6] Shook, C.A., and Roco, M.C., *Slurry Flow: Principles and Practice*, Butterworth-Heinemann, Boston, 1991.
- [7] Saxena, S.C., Patel, D., Smith, D.N., and Ruether, J.A., "An Assessment of Experimental Techniques for the Measurement of Bubble Size in a Bubble Slurry Reactor as Applied to Indirect Coal Liquefaction," *Chemical Engineering Communications*, **63**: 87-127 (1988).
- [8] Zhu, J.Y., "Laser Doppler Velocimetry for Flow Measurements in Pulp and Paper Research," *1996 Engineering Conference*, Chicago, TAPPI Press, 3-18 (September 16-19, 1996).
- [9] Walmsley, M.R.W., "Air Bubble Motion in Wood Pulp Fibre Suspension," *APPITA 1992 Proceedings*, 509-515 (1992).
- [10] Göttsching, L., Hunold, M., Krauthauf, T., Müller, J., and Putz, H.-J., "Effect of Air Volume and Air Bubble Size Distribution on Flotation in Injector Aerated Deinking Cells," *3rd Research Forum on Recycling*, Vancouver, BC, 17-25 (November 20-22, 1995).
- [11] Lindsay, J.D., Ghiaasiaan, S.M., and Abdel-Khalik, S.I., "Macroscopic Flow Structure in a Bubbling Paper Pulp-Water Slurry," *Industrial and Engineering Chemistry Research*, **34**: 3342-3354 (1995).
- [12] Physics International, "Flash X-ray Seminar," Flash X-ray Seminar, San Leandro, CA (1996).
- [13] Jamet, F., and Thomer, G., *Flash Radiography*, Elsevier Publishing Company, Inc., New York, 1976.
- [14] Cartz, L., *Nondestructive Testing*, ASM International, Materials Park, OH, 1995.
- [15] Bennett, A.W., Hewitt, G.F., Kearsy, H.A., Keeys, R.K.F., and Lacey, P.M.C., "Flow Visualization Studies of Boiling at High Pressure," *Proceedings of the Institution of Mechanical Engineers, Part 3C*, **180**: 1-11 (1965).
- [16] Hewitt, G.F., and Roberts, D.N., "Studies of Two-Phase Flow Patterns by Simultaneous X-ray and Flash Photography," United Kingdom Atomic Energy Authority (UKAEA), Harwell, Berkshire, Report Number: AERE-M2159, (1969).
- [17] Rowe, P.N., and Partridge, B.A., "An X-ray Study of Bubbles in Fluidised Beds," *Transactions of the Institute of Chemical Engineers*, **43**: T157-T175 (1965).
- [18] Farrington, T.E., Jr., "A More Fundamental Approach to the Problem of High Consistency Forming," *1986 TAPPI Engineering Conference*, Atlanta, GA, TAPPI PRESS, 709-717 (September 22-25, 1986).
- [19] Farrington, T.E., Jr., "Soft X-ray Imaging Can Be Used To Assess Sheet Formation and Quality," *TAPPI Journal*, **71**(5): 140-144 (1988).
- [20] Farrington, T.E., Jr., "Flash X-ray Imaging of Kraft Black Liquor Sprays," *TAPPI Journal*, **71**(2): 89-92 (1988).
- [21] Triantafillopoulos, N.G., and Farrington, T.E., Jr., "Flash X-ray Radiography Techniques for Visualizing Coating Flows," *1988 TAPPI Coating Conference*, New Orleans, LA, TAPPI PRESS, 47-52 (May 8-12, 1988).
- [22] Zavaglia, J.C., and Lindsay, J.D., "Flash X-ray Visualization of Multiphase Flow During Impulse Drying," *TAPPI Journal*, **72**(9): 79-85 (1989).
- [23] Monefeldt, J.L., "Flow Structures in a Quiescent Rectangular Bubble Column," MS Thesis, Institute of Paper Science and Technology, Atlanta, GA (1996).
- [24] TAPPI, "T 205 om-88 - Forming Handsheets for Physical Tests of Pulp," *TAPPI Test Methods 1994-1995*, Atlanta, TAPPI PRESS, (1994).

- [25] Hewitt, G.F., "Flow Regimes," *Handbook of Multiphase Systems*. G. Hetsroni, Ed. New York, Hemisphere Publishing Corp., Chapter 2.1 (1982).
- [26] Fallows, J.D., "Flotation Deinking," *Deinking Seminar (Atlanta) Notes*, Atlanta, GA, TAPPI PRESS (June 22-24, 1992).
- [27] Treybal, R.E., *Mass-Transfer Operations*, McGraw-Hill, New York, 1980.

ACKNOWLEDGMENTS

Financial support of this work by the Institute of Paper Science and Technology and its Member Companies is gratefully acknowledged. Portions of this work were used by James Monefeldt in partial fulfillment of the requirements for the M.S. degree at the Institute of Paper Science and Technology. Special thanks is extended to Paul Phelan for FXR training and troubleshooting. Additionally, the help of Adele Emery with digitizing the radiographs for presentation purposes is gratefully acknowledged.

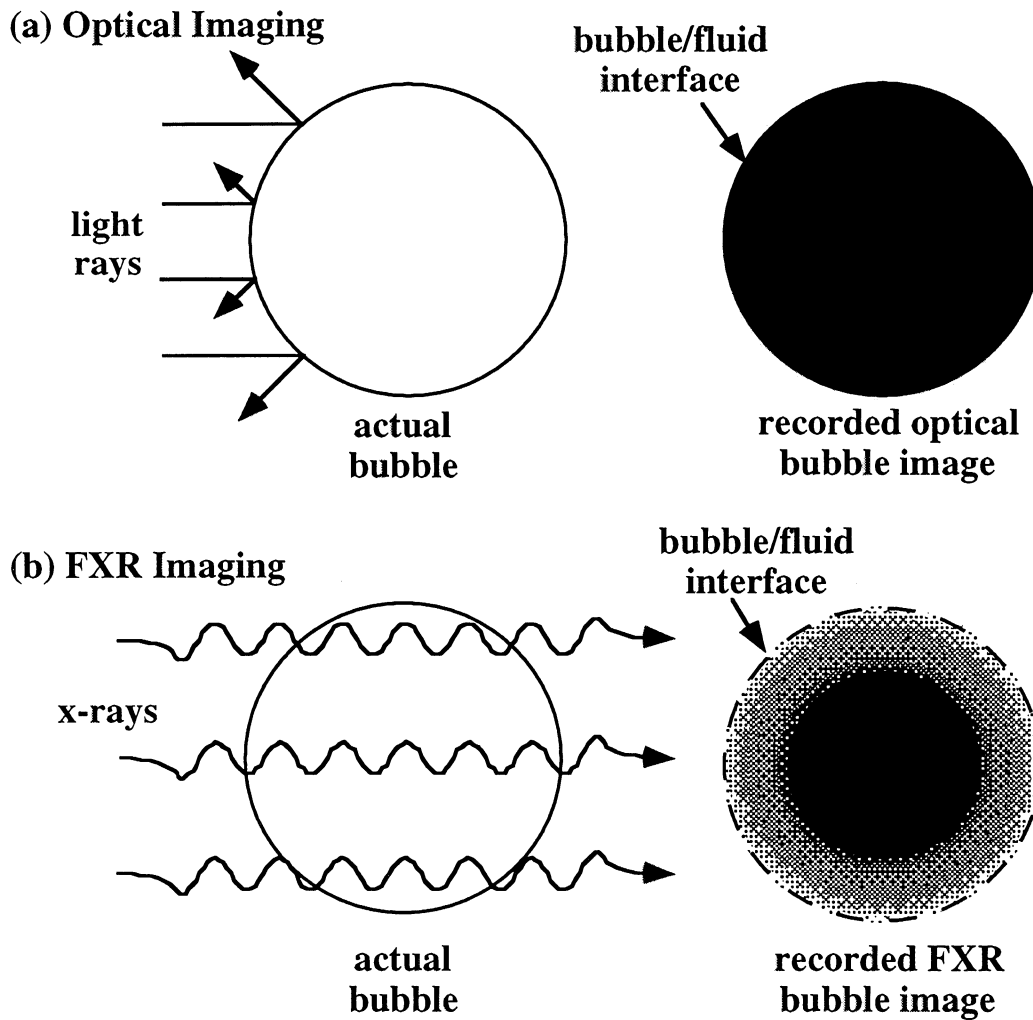


Fig. 1: Schematic representation of (a) optical and (b) flash x-ray radiography (FXR) imaging techniques.

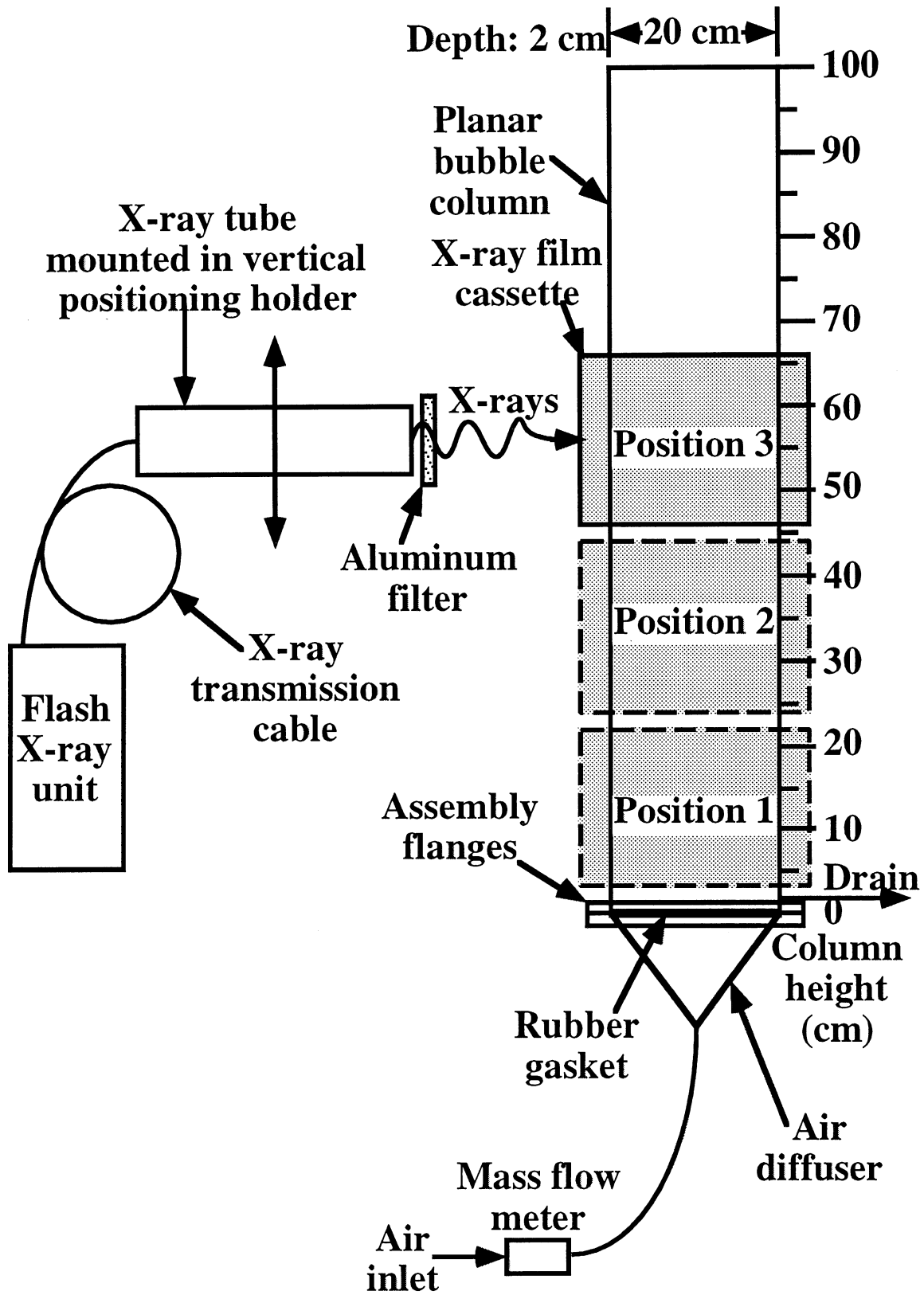


Fig. 2: Schematic diagram of the flash x-ray radiography experimental set up.

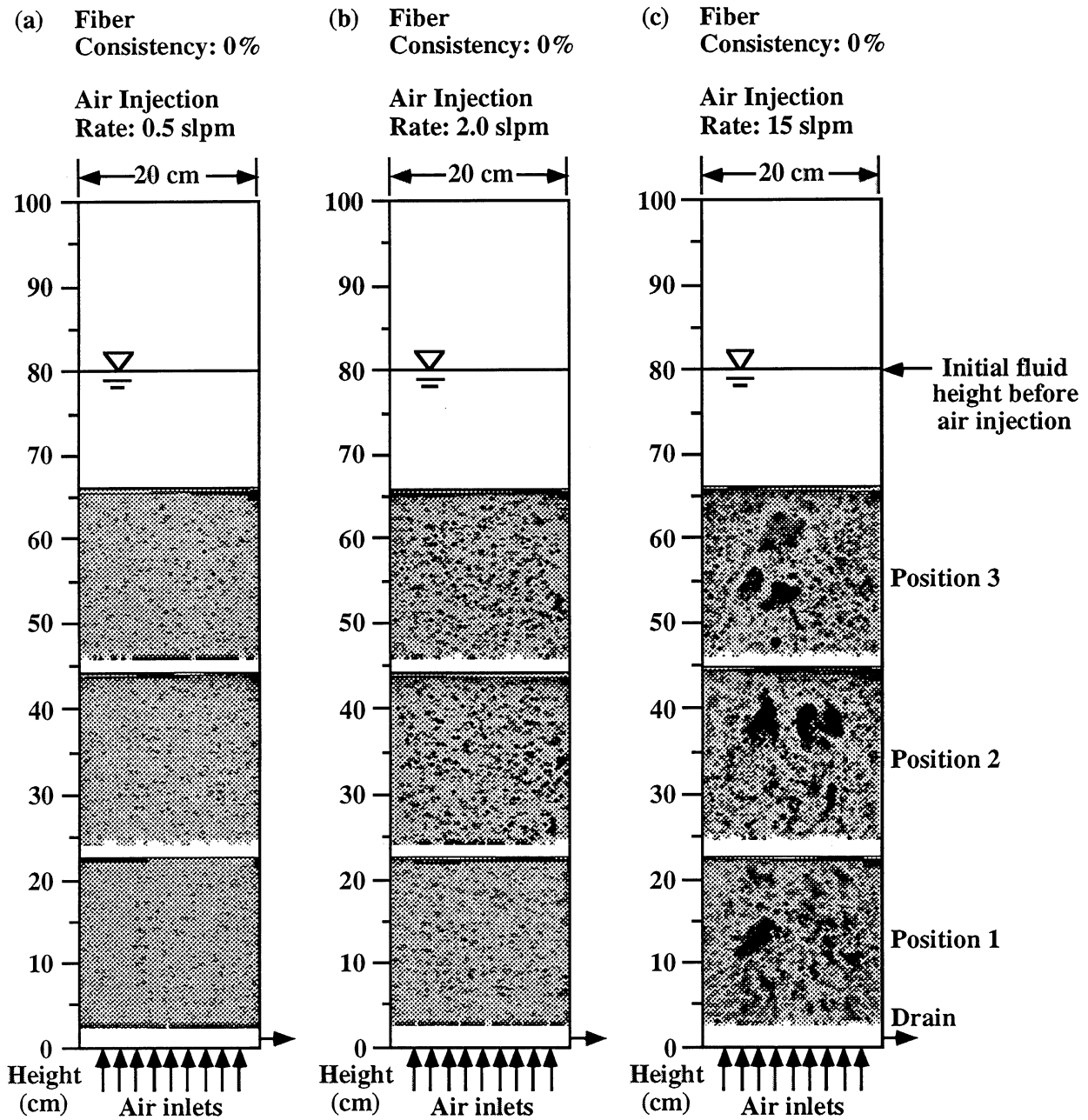


Fig. 3: Radiographs of the bubble flow patterns (the dark areas represent air bubbles) in an air/water system at air injection rates of (a) 0.5 slpm, (b) 2.0 slpm, and (c) 15 slpm.

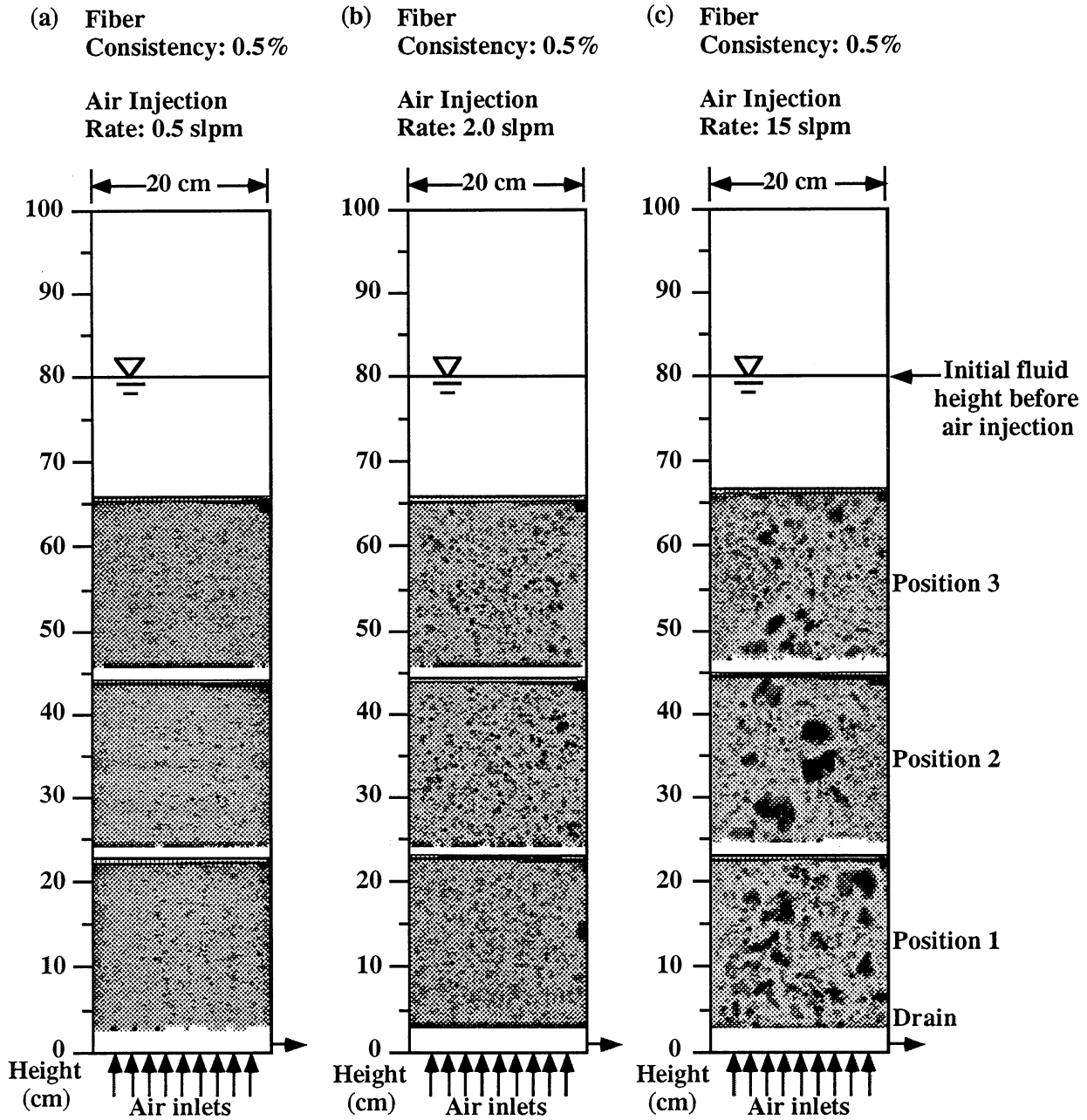


Fig. 4: Radiographs of the bubble flow patterns (the dark areas represent air bubbles) in an air/water/0.5% ONP system at air injection rates of (a) 0.5 slpm, (b) 2.0 slpm, and (c) 15 slpm.

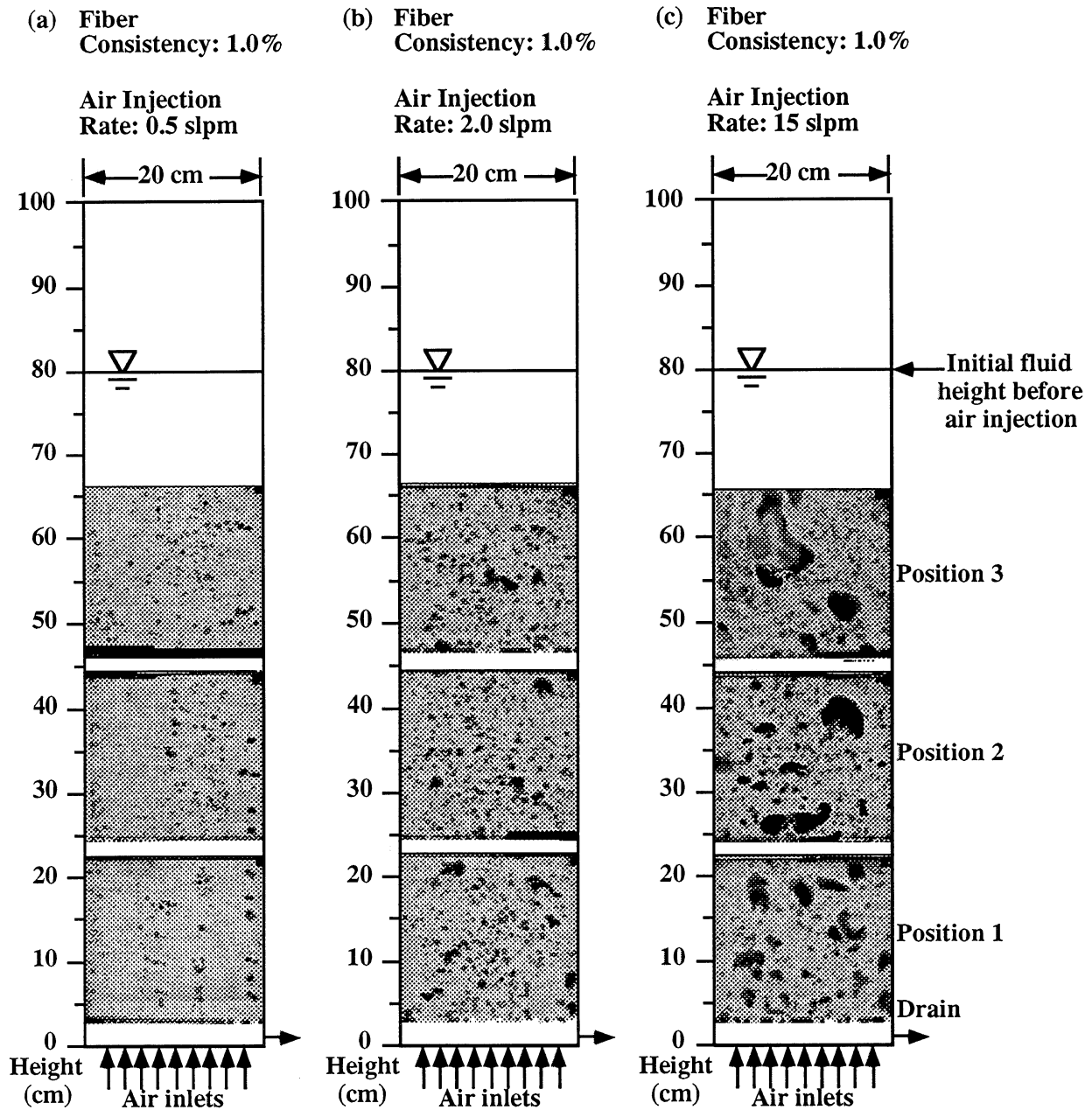


Fig. 5: Radiographs of the bubble flow patterns (the dark areas represent air bubbles) in an air/water/1.0% ONP system at air injection rates of (a) 0.5 slpm, (b) 2.0 slpm, and (c) 15 slpm.

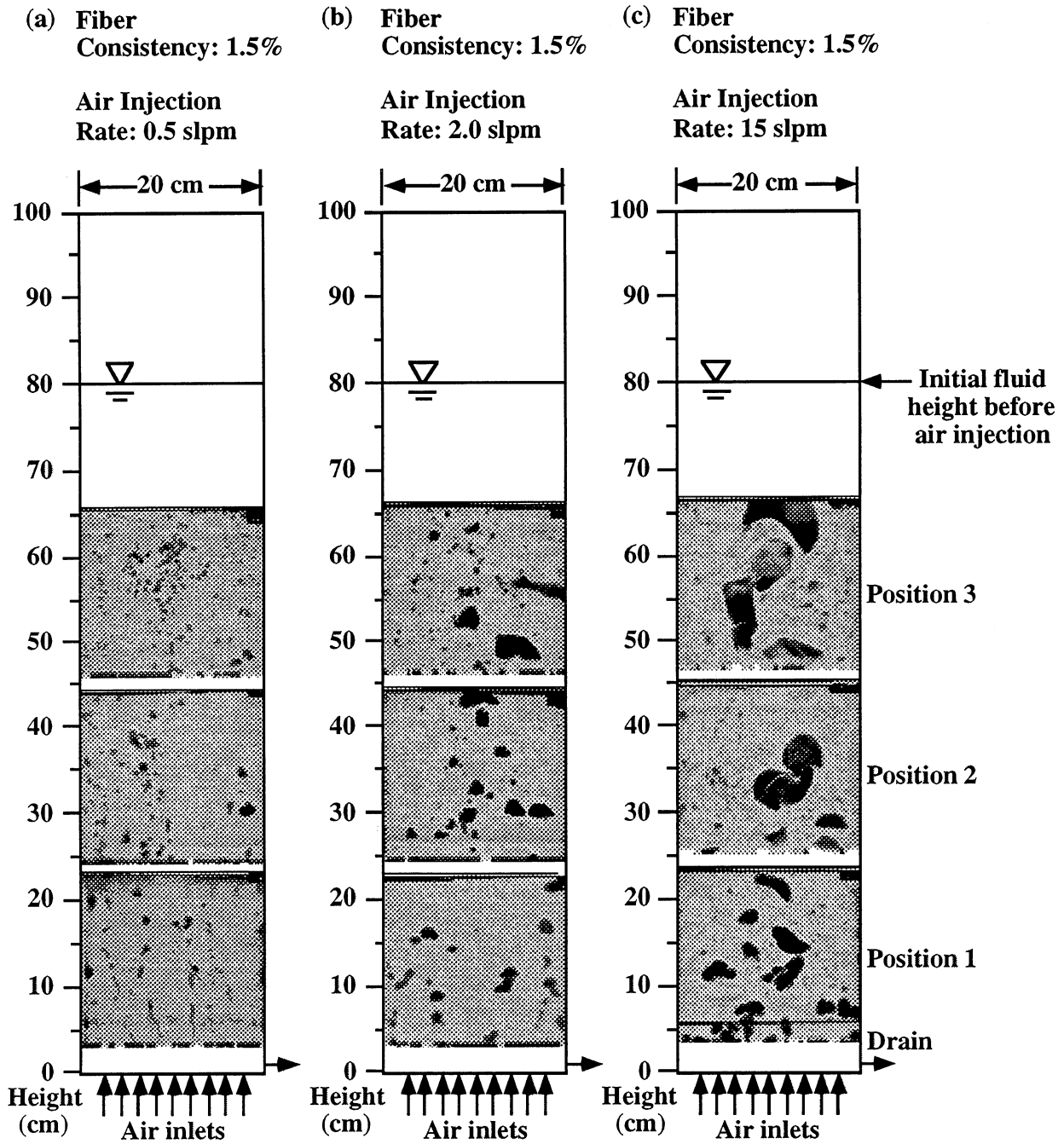


Fig. 6: Radiographs of the bubble flow patterns (the dark areas represent air bubbles) in an air/water/1.5% ONP system at air injection rates of (a) 0.5 slpm, (b) 2.0 slpm, and (c) 15 slpm.

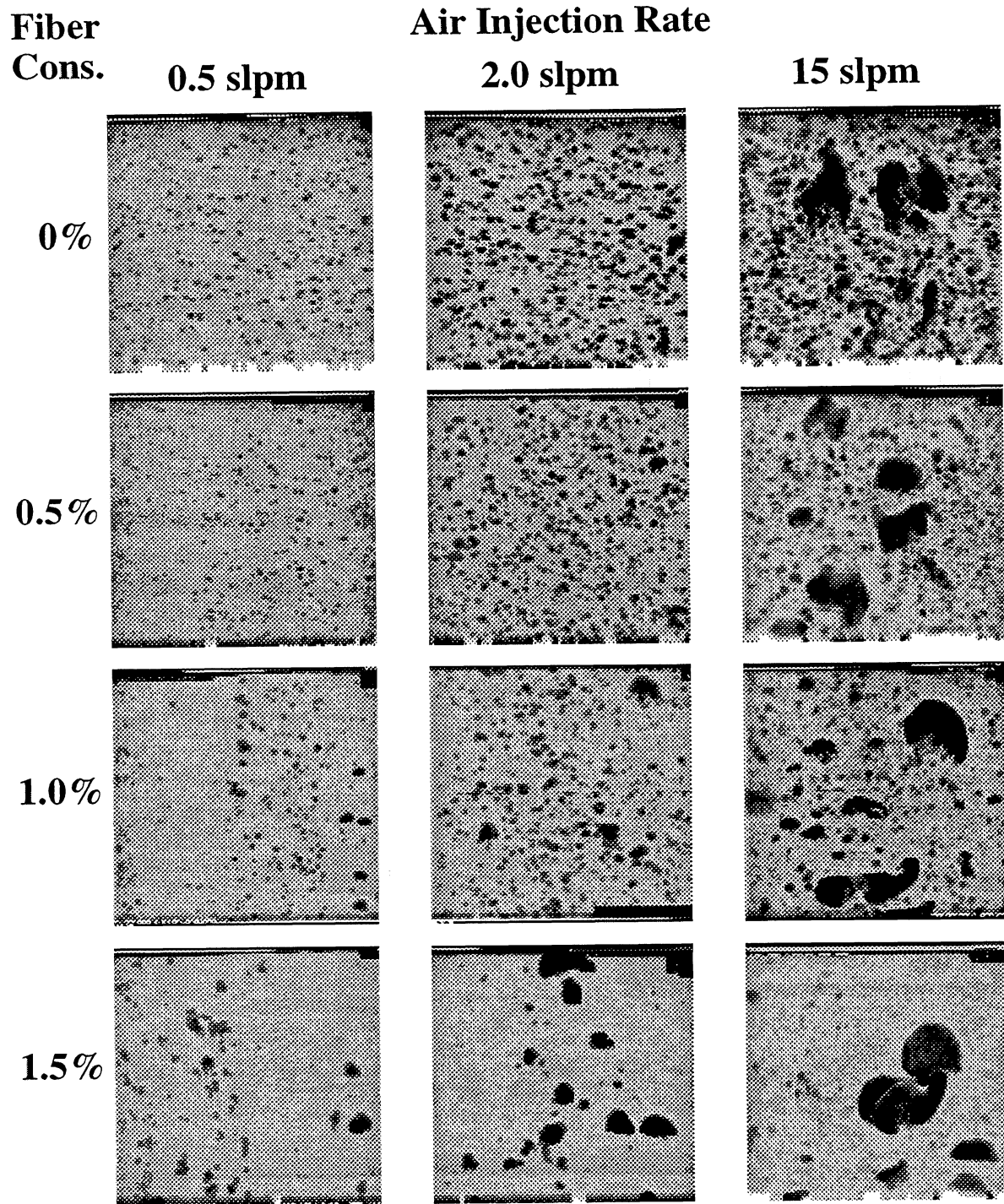


Fig. 7: Radiograph comparisons taken at Position 2 for various air injection rates and ONP consistencies.

